ENVIRONMENTAL RESEARCH
LETTERS

PAPER • OPEN ACCESS

Seasonality buffers carbon budget variability across heterogeneous landscapes in Alaskan Arctic tundra

ENVIRONMENTAL RESEARCH
LETTERS

CrossMark

OPEN ACCESS

RECEIVED
20 October 2020

REVISED
1 February 2021

ACCEPTED FOR PUBLICATION
3 February 2021

PUBLISHED
22 February 2021

LETTER

Seasonality buffers carbon budget variability across heterogeneous landscapes in Alaskan Arctic tundra

Josh Hashemi[1,2], Donatella Zona[2,3], Kyle A Arndt[4], Aram Kalhori[5] and Walter C Oechel[2,6]

[1] Department of Land, Air and Water Resources, University of California at Davis, Davis, United States of America
[2] Biology Department, San Diego State University, San Diego, United States of America
[3] Department of Animal and Plant Sciences, University of Sheffield, Sheffield, United Kingdom
[4] Earth Systems Research Center, Institute for the Study of Earth, Oceans, and Space, University of New Hampshire, Durham, United States of America
[5] GFZ German Research Centre for Geosciences, Potsdam, Germany
[6] Department of Geography, College of Life and Environmental Sciences, University of Exeter, Exeter, United Kingdom

E-mail: jfhashemi@ucdavis.edu

Keywords: Arctic tundra, carbon budget, eddy covariance, landscape heterogeneity, seasonality

Supplementary material for this article is available online

Abstract

Arctic tundra exhibits large landscape heterogeneity in microtopography, hydrology, and active layer depth. While many carbon flux measurements and experiments are done at or below the mesoscale ($\leqslant$1 km), modern ecosystem carbon modeling is often done at scales of 0.25°–1.0° latitude, creating a mismatch between processes, process input data, and verification data. Here we arrange the naturally complex terrain into mesoscale landscape types of varying microtopography and moisture status to evaluate how landscape types differ in terms of CO_2 and CH_4 balances and their combined warming potential, expressed as CO_2 equivalents (CO_2-eq). Using a continuous 4 year dataset of CO_2 and CH_4 fluxes obtained from three eddy covariance (EC) towers, we investigate the integrated dynamics of landscape type, vegetation community, moisture regime, and season on net CO_2 and CH_4 fluxes. EC towers were situated across a moisture gradient including a moist upland tundra, a heterogeneous polygon tundra, and an inundated drained lake basin. We show that seasonal shifts in carbon emissions buffer annual carbon budget differences caused by site variability. Of note, high growing season gross primary productivity leads to higher fall zero-curtain CO_2 emissions, reducing both variability in annual budgets and carbon sink strength of more productive sites. Alternatively, fall zero-curtain CH_4 emissions are equal across landscape types, indicating site variation has little effect on CH_4 emissions during the fall despite large differences during the growing season. We find that the polygon site has the largest mean warming potential (107 ± 8.63 g C–CO_2-eq m^{-2} yr^{-1}) followed by the drained lake basin site (82.12 ± 9.85 g C–CO_2-eq m^{-2} yr^{-1}) and the upland site (77.19 ± 21.8 g C–CO_2-eq m^{-2} yr^{-1}), albeit differences were not significant. The highest temperature sensitivities are also at the polygon site with mixed results between CO_2 and CH_4 at the other sites. Results show a similar mean annual net warming effect across dominant landscape types but that these landscape types vary significantly in the amounts and timing of CO_2 and CH_4 fluxes.

1. Introduction

Arctic tundra is characterized by long non-growing periods punctuated with short growing seasons and a high degree of landscape heterogeneity caused by freeze-thaw cycles. Because these ecosystems are largely inundated or frozen for much of year, soil decomposition is slow, resulting in one of the largest terrestrial reservoirs of labile carbon (C) (Hugelius *et al* 2014). Comprising only 15% of the global land surface, Arctic tundra contain close to one third of the Earth's terrestrial soil C (∼1500 Pg-C) (Zimov *et al* 2006, Tarnocai *et al* 2009, Kirschke *et al* 2013). As this region is undergoing accelerated warming (Serreze and Francis 2006), carbon dioxide (CO_2) emissions are increasing, causing a sink-source transition (Schuur *et al* 2013, Oechel *et al* 2014, Natali *et al* 2015, 2019, Commane *et al* 2017). In addition to CO_2, methane (CH_4) is an important greenhouse gas (GHG) in permafrost and wetland regions as methanogens thrive in areas with large amounts of anaerobic soil (Garcia *et al* 2000). Arctic wetlands are responsible for ∼15% of global wetland CH_4 emissions and ∼4% of all global CH_4 emissions (Kirschke 2013). As methanogenesis is a temperature sensitive process (Dunfield *et al* 1993), it is likely that biogenic CH_4 emissions will increase (Tian *et al* 2012, Lawrence *et al* 2015). For this reason, attention to natural sources of CH_4 efflux has increased in Arctic regions.

Landscape heterogeneity can contribute to the wide range of estimates in CH_4 emission, ecosystem respiration (ER), and gross primary productivity (GPP) (McGuire *et al* 2012, Treat *et al* 2018b). This heterogeneity is characterized by variability in soil moisture regime and develops from freeze-thaw cycles into a patchwork of polygonized tundra, thaw lakes, drained lake basins and moist upland tundra (Webber 1978, Zulueta *et al* 2011, Liljedahl *et al* 2016). Polygonized tundra occurs from the common development of ice wedges in the soil column. As ice wedges degrade, inundated C rich low-centered polygons become drained high-centered polygons and drier upland tundra (Liljedahl *et al* 2016). This shift can cause a decrease in CH_4 emissions and an increase in CO_2 emissions (Martin *et al* 2018). Degrading ice wedges can also form trough ponds that facilitate water movement, change the microbial community and, by extension, change GHG fluxes (Koch *et al* 2014, Liljedahl *et al* 2016). Similarly, thaw lakes form from permafrost thawing and subsequent land subsidence (Jorgensen and Shur 2007, Huissteden *et al* 2011). Thaw lakes drain, forming vegetated drained lake basins (Jorgenson and Shur 2007). This indicates that over short distances, the effects of climate change and controls of emissions can be highly variable due to soil moisture content and the resulting plant and microbial communities that develop.

Recent studies have shown emissions of CO_2 and CH_4 occur well into the non-growing season (Euskirchen *et al* 2012, Oechel *et al* 2014, Zona *et al* 2016, Treat *et al* 2018a, Arndt *et al* 2019a). Cold period emissions of CH_4 can account for nearly 50% of the yearly budget, and largely occur during fall shoulder periods when air and surface soil temperatures are below freezing, and subsurface temperatures are around 0 °C (20%–30%) (Zona *et al* 2016, Commane *et al* 2017, Taylor *et al* 2018). This period is referred to as the 'zero-curtain' and is associated with the presence of an unfrozen portion of the active layer during freezing while phase transition occurs (Outcalt *et al* 1990). This highlights the importance of seasonality, yet there is still a paucity of data reflecting how interseasonal C dynamics vary in terms of landscape type.

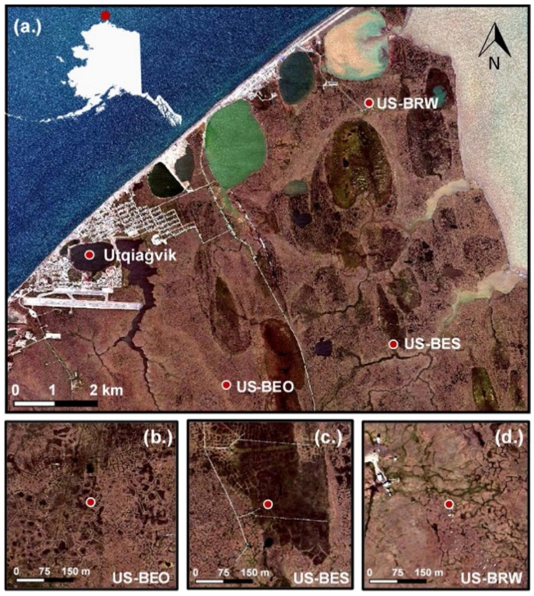

Figure 1. WorldView-3 (Maxar Technologies) imagery acquired 24, July 2016 of Utqiaġvik, AK (a) and the three eddy-covariance experimental sites, US-Beo (b), US-Bes (c), and US-Brw (d). Images generated using Environment for Visualizing Images V5.5 (Harris Geospatial) software.

Quantifying ongoing changes to the pan-Arctic carbon budget is important, but cannot be achieved without understanding how variability in landscape scale climate responses affect emissions. By partitioning Arctic tundra ecosystems into sub-landscapes, the variability in timing and magnitude of C fluxes can be better understood. Using a continuous 4 year dataset (2014–2017) of CO_2 and CH_4 fluxes obtained from three eddy covariance (EC) towers, each in a distinct landscape type, this study aims to quantify the integrated dynamics involved in CH_4, CO_2, and $CO_2 + CH_4$ (expressed as CO_2 equivalent (CO_2-eq), hereafter referred to as combined C) budgetary contributions due to landscape type, vegetation community composition, and seasonality.

2. Methodology

2.1. Study area

EC study sites are located on continuous permafrost tundra on the North Slope of Alaska, near Utqiaġvik (figure 1(a)). The sites include the Barrow Environmental Observatory (US-Beo) (figure 1(b)), Biocomplexity Experiment South (US-Bes) (figure 1(c)) and a site near the NOAA Earth System Research Laboratory (US-Brw) (figure 1(d)). These sites were chosen for long-term continuous data acquisition as they capture dominant landscape variability of the region. US-Bes is in a drained lake basin containing the wettest soils (table 1), with the water table above the surface for most of the growing season and is dominated by wet sedges and sphagnum moss (Davidson *et al* 2016a). US-Brw is a moist upland tundra containing the driest soils (table 1) and is dominated by

Table 1. Instrumentation and site information.

Site	Coordinates	Data DOI	EC height	GGA	Anemometer	MMTD	SWC
US-Brw	71.322 N −156.609 W	10.18739/A2X34MS1B	4.2 m	LGR FGGA	METEK uSonic3 Class A	57 ± 8 cm	47% ± 4%
US-Beo	71.281 N −156.612 W	10.18739/A2X34MS1B	3.1 m	LGR FGGA	Campbell scientific CSAT3	60 ± 6 cm	H: 59% ± 10% T: 72% ± 18%
US-Bes	71.280 N −156.596 W	10.18739/A2X34MS1B	2.2 m	LGR FGGA	Campbell scientific CSAT3	44 ± 5 cm	83% ± 12%

Abbreviations: LGR FGGA—Los Gatos Research Fast Greenhouse Gas Analyzer; MMTD—mean maximum thaw depth; SWC—soil water content (H—high center, T—trough). Values represent mean ± standard error over the study period.

graminoids and lichens (Kwon *et al* 2006). US-Beo is characterized by ice wedge polygon formations that arise from the freeze thaw cycle (Webber 1978). Due to these polygon formations, US-Beo is a mixed landscape, exhibiting both inundated and drained areas and consists of wet sedge/sphagnum moss dominated areas as well as drier graminoid/lichen dominated areas (Davidson *et al* 2016a).

2.2. Eddy covariance and meteorological data

CH_4 and CO_2 fluxes were estimated at half-hourly intervals from year-round data collected at 10 Hz following the procedures outlined from LI-COR® EddyPro®. A double rotation was applied to the axis rotations of three-dimensional wind speeds according to Wilczak *et al* (2001) and a block averaging interval was used to define turbulent fluctuations. An in situ/analytic correction, according to Ibrom *et al* (2007), was applied to the gas analyzer data as the greenhouse gas analyzer (GGA) has a closed path. Quality flags were output within datasets according to Mauder and Foken (2011) and data that did not pass the quality requirements were removed. An internal chamber pressure of $\geqslant$20.67 kPa (155 torr) in the GGA indicates line blockage or instrument failure, and these data were eliminated. Additionally, a turbulence threshold was applied, identifying conditions with insufficient turbulence (indicated by low friction velocity ($u^* \leqslant 0.1$ m s^{-1})), and those data were removed in accordance with Reichstein *et al* (2005). A moving window of 2 weeks was applied and fluxes that were three standard deviations away from the mean were removed as outliers for CH_4 and CO_2 fluxes. EC tower site and instrumentation information can be found in table 1 (Goodrich *et al* 2016, Arndt *et al* 2020).

Meteorological data were obtained at 30 s intervals and averaged into half-hourly means. Each of the three sites had independent meteorological instrumentation and measurements used in defining the peak thaw and zero-curtain period. Meteorological instrumentation used in analysis included soil water content (SWC) (Campbell Scientific® CS616 Water Content Reflectometer), soil temperature (Omega Engineering™, type T thermocouples), air temperature and humidity (Vaisala, HMP 45), and photosynthetically active radiation (PAR; LI-COR® LI-190R quantum sensor). At each site, soil temperature was measured at 0, −5, −15, and −30 cm from the soil surface and soil moisture probes were inserted from the soil surface to a depth of 20 cm, providing the average soil moisture in the top 20 cm of the soil column. Measurements of soil moisture were taken at one location at US-Brw and US-Bes, and two locations at US-Beo (a high center polygon and polygon trough) for better relief representation then averaged over the growing seasons within the study period. Data from both EC and meteorological instrumentation were collected using datalogger/multiplexer arrays from Campbell Scientific® (i.e. CR-3000, CR-23X and AM-1632). Thaw depth was measured weekly during the growing season by probing the land surface to the extent of the active layer along a transect with a small diameter metal rod.

2.3. Data/statistical analyses

EC tower footprints were estimated with the analytical footprint model of Korman and Meixner (KM) (2001) using the R package 'FReddyPro' v1.0 (Xenakis 2016). The KM model calculates the density function of the footprint contribution for a two-dimensional area surrounding the EC tower and was used to estimate the landscape area in which 80% of fluxes originated by averaging half-hourly single flux footprints during 2016. WorldView-3 (Maxar Technologies) imagery (1.24 m multispectral resolution) of Utqiaġvik, AK was used to show variability in the WorldView normalized difference water index (NDWI) at each of the three sites. As SWC is measured at one to two locations within each EC tower footprint and site hydrology can be variable, NDWI is used in conjunction with SWC to characterize differences in site moisture regime. The WorldView NDWI is calculated as the normalized difference between the coastal band (R_c, 400–450 nm) reflectance and the second near infrared band (R_{NIR2}, 860–1040 nm) reflectance (equation (1)). This is because it has been shown that the R_c and R_{NIR2} bands show a better soil-water separation than the typical green (510–580 nm) and the first near infrared band (770–895 nm) combinations and is indicative of surface water moisture levels (Maglione *et al* 2014). The NDWI results in values between −1 and 1 where more positive values represent wetter landscapes. Pixels outside of the footprint of the EC towers as well as those representing structures within the tower footprints were masked for statistical analysis. Before calculating statistics, pixels were aggregated into 3 × 3 pixel grids using the nearest neighbor approach to avoid bias by over sampling and to reduce high variability. A pairwise Wilcoxon rank sum tests was used to compare NDWI values among sites. Additional imagery for NDWI analysis across study period can be found in supplementary information (figure S1 (available online at stacks.iop.org/ERL/16/035008/mmedia))

$$\mathrm{NDWI} = \frac{R_C - R_{NIR2}}{R_C + R_{NIR2}}. \quad (1)$$

Daily average fluxes were calculated in R V 3.6.2 (R Core Team 2019) and R Studio software using the 'data.table' package and were calculated with a minimum of 30 half-hourly samples per day to ensure proper representation of the diurnal patterns of CH_4 and CO_2 fluxes. Daily averages of CH_4 and CO_2 fluxes for purposes of the examination of site variability and C budgets are beneficial as they show an accurate representation of the systems while qualifying data complexity and size. Data gaps are unavoidable in the harsh conditions characteristic of Arctic environments. These gaps can be a result of power or network outages as well as instrument failure. Total data coverage is between 61% and 71% depending on the site with the best coverage during the summer and fall periods. Detailed data coverage information by season and annual totals can be found in the supporting information (table S1). Data gaps were filled using random forest machine learning (R package, 'missForest') utilizing a 300-decision tree design. Model validation can be found in supporting information (figure S2). Comparisons of model validation between the default half-hourly data output and daily averages show models perform much better when using a daily average. This method reduces the 'noise' and is therefore better equipped to inform machine learning processes.

The beginning of the growing season was defined as the period where the top five cm of the soil are above 0 °C, ending at the onset of the zero-curtain. The zero-curtain was defined as the period during the fall shoulder beginning when soil temperature of the top 5 cm of the soil are less than 0 °C for 3 or more days, ending when the temperature at −15 cm (roughly the middle of the active layer, table 1) dropped below −0.75 °C for 3 or more days. Non-growing season, as defined here, includes both winter and spring, beginning at the end of the zero-curtain period and ending at the beginning of the growing season.

ER and GPP were partitioned from net ecosystem exchange (NEE) according to Lasslop *et al* (2010) using the 'REddyproc' package in R (Wutzler *et al* 2018), as nighttime data is unobtainable during Arctic summer. Temperature response relationships were calculated using a weekly mean to reduce noise and to better represent annual trends. Models showing temperature response curves for CH_4 were calculated using soil temperature, rather than air temperature, as this has been shown to act as a better predictor for CH_4 fluxes (Arndt *et al* 2019a) (figure S3). All temperature response curves were linearized by log transformation and compared using analyses of covariance (ANCOVA) to test for homogeneity among the regressions with the 'car' R package (Fox and Weisberg 2019) and Q_{10} values were calculated from temperature response regressions with the 'respirometry' R package (Birk 2020).

3. Results

3.1. Site moisture regime

NDWI as well as the KM model footprint of each EC tower were used to establish differences in surface water content within each EC tower footprint (figure 2). Using a pairwise Wilcoxon rank sum tests, NDWI was found to be significantly different ($p < 0.001$) among each of the three sites. The results of the NDWI, showing levels of surface moisture, agreed with soil moisture data at the sites (table 1) with US-Bes showing the wettest conditions (NDWI (mean ± standard error) = −0.079 ± 0.005), US-Beo showing intermediate NDWI levels (NDWI = −0.144 ± 0.003) and US-Brw with the lowest NDWI supporting its position as the driest site in the study (NDWI = −0.204 ± 0.003). Further analyses of NDWI show that imagery acquired 24 July 2016 was representative of site differences and while some variability occurs, these positions are maintained (figure S1) as changes in vegetation community or hydrology at the landscape scale happens over longer periods of time (Liljedahl *et al* 2016, Arndt *et al* 2019b).

3.2. Seasonal gas flux

Peak growing season CH_4 emissions were higher at US-Bes (1.43 ± 0.11 mg C–CH_4 m^{-2} h^{-1}) and US-Beo (1.35 ± 0.31 mg C–CH_4 m^{-2} h^{-1}) in comparison with US-Brw (0.76 ± 0.10 mg C–CH_4 m^{-2} h^{-1}), however, CH_4 fluxes during the zero-curtain period showed lower variability across the three study sites (figure 3(a)). The annual average of peak uptake in NEE was greatest at the driest site, US-Brw (75.26 ± 8.9 mg C–CO_2 m^{-2} h^{-1}), followed by US-Beo (60.5 ± 7.9 mg C–CO_2 m^{-2} h^{-1}) and least pronounced at wettest site, US-Bes (39 ± 6.4 mg C–CO_2 m^{-2} h^{-1}). The annual average of peak emission in NEE followed the same order of US-Brw (44.25 ± 4.9 mg C–CO_2 m^{-2} h^{-1}), US-Beo (24.74 ± 5.3 mg C–CO_2 m^{-2} h^{-1}) and US-Bes (13.75 ± 1.7 mg C–CO_2 m^{-2} h^{-1}) (figure 3(b)).

3.3. Carbon budget variability

Seasonal fluctuations (growing season to zero-curtain) of CO_2 budgets are most pronounced at the driest site, US-Brw, and least pronounced at wettest site, US-Bes (figure 4(a)). Due to the higher zero-curtain CO_2 emissions dampening growing season CO_2 uptake, US-Brw is the weakest CO_2 sink on average. This trend holds with drier sites generally emitting larger amounts of CO_2 during the zero-curtain offsetting much of the uptake during the growing season (US-Brw: 75%; US-Beo: 62%; US-Bes: 25%). Growing season CH_4 emissions are highest at US-Beo and US-Bes (figure 4(b), $p < 0.05$). However, zero-curtain CH_4 emissions are roughly equal across all landscapes. This indicates that the percent contribution to local CH_4 budget varies by site during the zero-curtain (US-Brw: 45%; US-Beo: 34%; US-Bes: 32%) and total non-growing season (US-Brw: 56%; US-Beo: 48%; US-Bes: 43%).

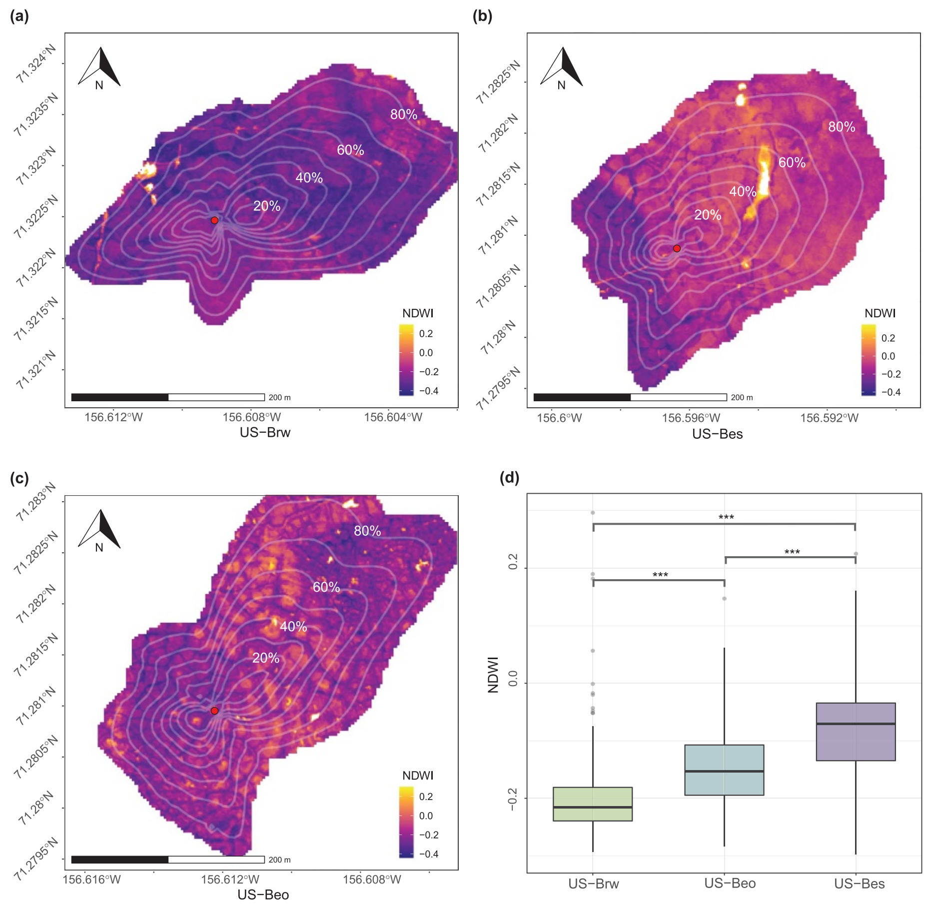

Figure 2. NDWI within EC tower footprints at (a) US-Brw, (b) US-Bes, and (c) US-Brw and NDWI by site (d). Red circles represent EC Tower and isolines are at each 10% and represent cumulative percent of flux contribution. (***$p < 0.001$). WorldView-3 (Maxar Technologies) imagery acquired 24 July 2016 of Utqiaġvik, AK.

Site variability in combined C budgets are most pronounced during the growing season, yet still occur, driven by CO_2 emission, during the zero-curtain period (figure 4(c)). As US-Beo is characterized by low centered polygons, it exhibits characteristics of both US-Brw and US-Bes. This accounts for the larger values observed in CH_4 emission relative to US-Brw and the larger values in net CO_2 uptake relative to US-Bes during the growing season. The effect is that the mixed landscape, US-Beo, is the largest mean C contributor (table 2). More detailed information regarding C budget by year/season can be found in supplementary information (table S2).

Yearly cumulative emissions indicate that interannual variability in CH_4 fluxes is limited in inundated sites (figure 5(a)). US-Bes exhibited the lowest interannual variability (standard deviation—CO_2-eq (σ) = 3.96), followed by US-Brw (σ = 15.2) then US-Beo (σ = 23.8). Interannual variability in CO_2 fluxes is highest at US-Brw (σ = 34.98), followed by US-Bes (σ = 18.11) then US-Beo (σ = 10.65) (figure 5(b)). Most of the variability in combined cumulative C emissions is therefore controlled by variability in CO_2 at US-Brw and US-Bes, and in CH_4 at US-Beo (figure 5(c)).

3.4. Temperature response rates

ER temperature response relationships show that air temperature increases in predictive strength as site wetness decreases (figures 6(a)–(c)). In the inter-site comparison of linearized ER regressions, US-Beo and US-Brw show significant similarity ($p < 0.05$) while US-Bes is significantly different than both US-Brw ($p = 0.12$) and US-Beo ($p = 0.076$). Q_{10} is highest at US-Beo (3.5), followed by US-Brw (2.5) and US-Bes (2.2). Methane temperature response relationships show similar predictive strength across all sites (figures 6(d)–(f)). Q_{10} for CH_4 is again highest at US-Beo (4.6), followed by US-Bes (4.2) and US-Brw (3.1). Contrary to ER, in the inter-site comparison of linearized CH_4 regressions, US-Beo and US-Bes show significant similarity ($p < 0.05$) while US-Brw is significantly different than both US-Beo ($p = 0.11$) and US-Bes ($p = 0.14$).

4. Discussion

4.1. CO_2 seasonality and annual budget

Seasonality appears to be the dominant factor in annual variation in NEE; however, we find the magnitude of that effect is dependent on local variation in site hydrology (figure 4). US-Brw exhibited

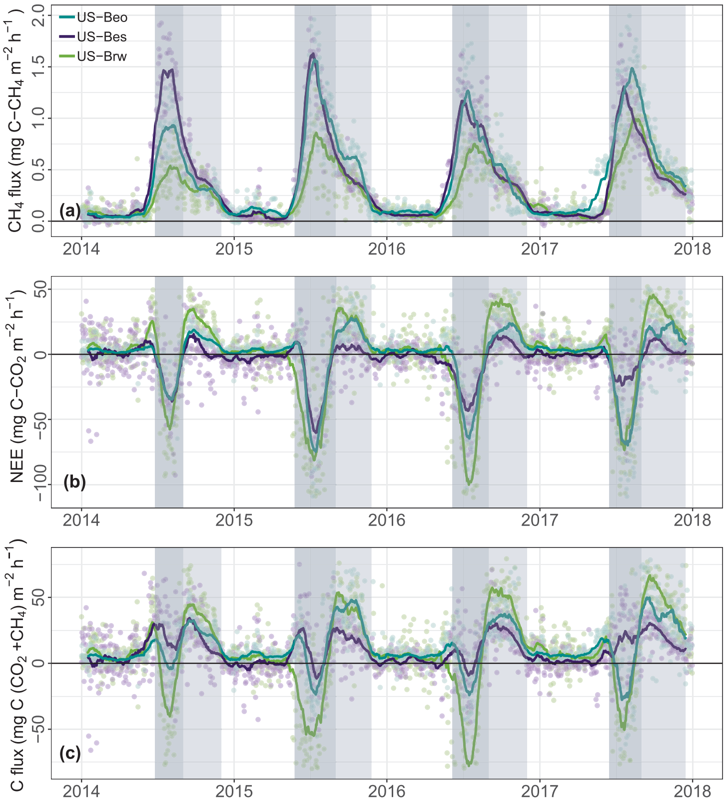

Figure 3. Carbon flux (daily average) of (a) CH_4, (b) CO_2 and (c) CO_2 + CH_4 (with CH_4 expressed as CO_2-eq based on warming potential) at the three EC sites. The darker shaded portion represents the growing season, while the lighter shaded portion represents the zero-curtain period.

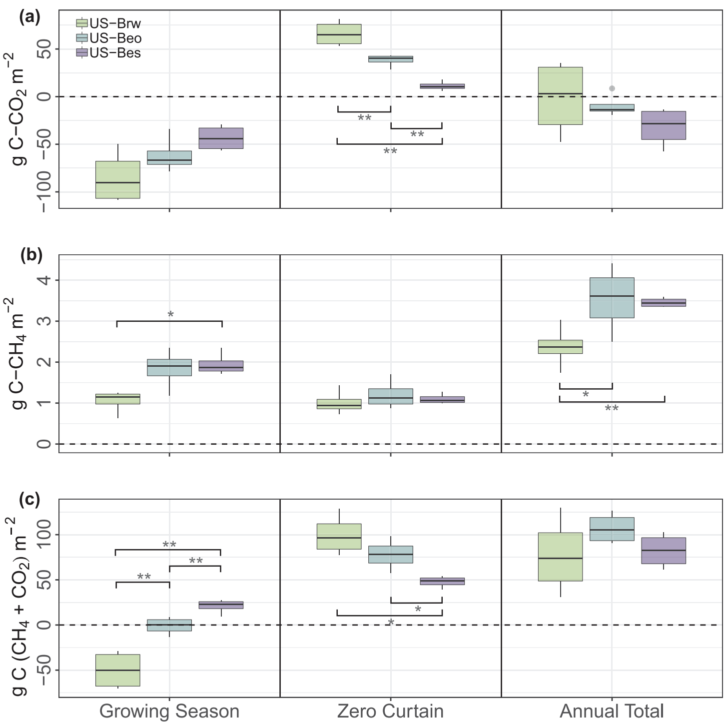

Figure 4. Seasonal and yearly budgetary contributions of (a) CO_2, (b) CH_4 and (c) CO_2 + CH_4 (expressed as CO_2-equivalent based on warming potential) at the three EC sites from the growing season, zero-curtain period, and yearly total ($^*p < 0.05$; $^{**}p < 0.01$).

Table 2. Mean seasonal and annual totals of NEE and CH_4 flux (g C m^{-2} season yr^{-1}).

	US-Brw			US-Beo			US-Bes		
Season	NEE	CH_4	C–C	NEE	CH_4	C–C	NEE	CH_4	C–C
Growing	−84.48 ± 12.2 GPP: −209.4 ± 24.9 ER: 125.4 ± 18.1	1.05 ± 0.12	−49.99 ± 10.8	−61.5 ± 8.3 GPP: −135 ± 12.4 ER: 74.6 ± 4.9	1.83 ± 0.21	−1.02 ± 4.86	−43.52 ± 5.9 GPP: −104.5 ± 7.8 ER: 62.7 ± 2.4	1.95 ± 0.12	20.75 ± 4
Zero-curtain	66.32 ± 5.9	1.01 ± 0.13	99.73 ± 11.51	38.24 ± 2.8	1.2 ± 0.15	77.92 ± 8.66	11.26 ± 2.1	1.11 ± 0.05	47.72 ± 3.27
Non-growing	16.69 ± 5.3	0.33 ± 0.04	27.45 ± 7.47	13.76 ± 1.1	0.5 ± 0.07	30.11 ± 3.82	0.33 ± 3.5	0.4 ± 0.07	13.68 ± 6.31
Annual	−1.47 ± 17.5	2.38 ± 0.23	77.19 ± 21.8	−9.5 ± 5.3	3.53 ± 0.36	107 ± 8.63	−31.93 ± 9.1	3.46 ± 0.05	82.12 ± 9.85

Note: values indicate mean ± standard error. Positive values indicate release to the atmosphere. C–C represents combined C.

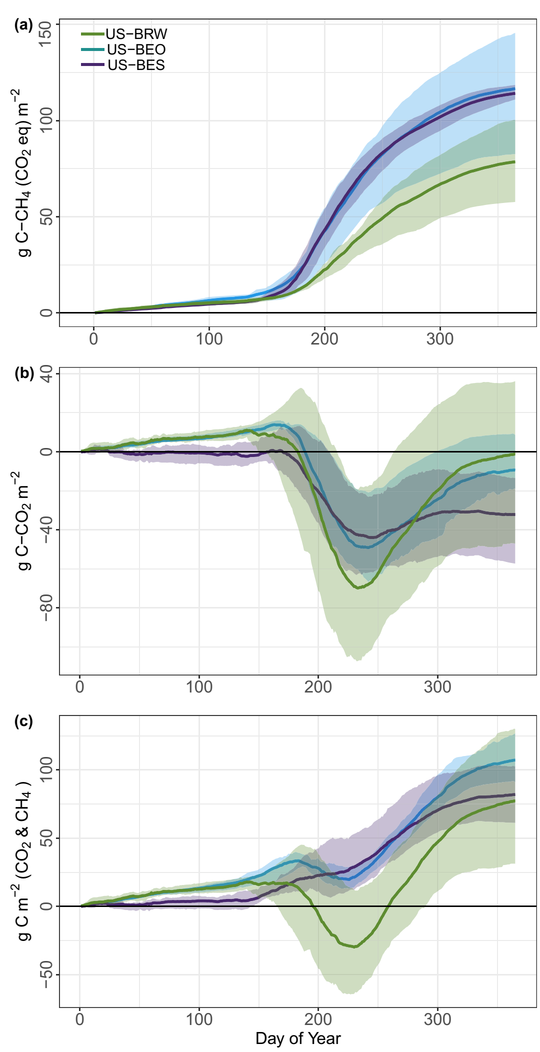

Figure 5. Mean annual cumulative emissions of (a) CH_4, (b) CO_2 and (c) $CO_2 + CH_4$ (with CH_4 expressed by a CO_2-equivalent) at the three EC sites. Shaded portion represents range of measurements across the 4 year study period.

the highest GPP yet was the weakest mean annual CO2 sink in comparison with the other wetter sites (table 2). Conversely, US-Bes exhibited the lowest GPP yet was the strongest mean annual CO2 sink (table 2). This is because sites with higher summer GPP exhibited larger zero-curtain CO2 emissions. The lower SWC at US-Brw likely leads to a substantially larger portion of the soil column under oxic conditions, therefore supporting aerobic respiration, increasing CO_2 emissions. While it is probable that this constitutes much of the budget disparity, the contribution of CH_4 oxidation to ER in primarily methanogenic areas has been found to be up to 35% (Nielsen *et al* 2019). As US-Brw contained the deepest active layer (table 1) and largest GPP (table 2), soils may contain higher amounts of photosynthates and labile C. This can increase methanogenesis rates deeper in the soil column (Dorodnikov *et al* 2011) and fuel CO2 producing methanotrophs closer to the surface that would be more active under the oxic conditions in drier areas relative to waterlogged areas (Megonigal and Schlesinger 2002). Alternatively, as US-Bes is inundated, methanotrophy is likely substantially lower during the zero-curtain period when the highest amount of CO2 loss is observed. Moreover, the lower GPP at US-Bes may result in more recalcitrant C and thus lower ER rates. The US-Beo site exhibited intermediate growing season GPP and zero-curtain CO2 emission relative to the other two sites likely due to US-Beo exhibiting a mixed landscape regarding the prevalence of drained and inundated areas (figure 4(a)).

ER temperature response relationships show that US-Beo had the strongest temperature dependence ($Q_{10} = 3.5$) relative to US-Brw and US-Bes ($Q_{10} = 2.5$ and $Q_{10} = 2.2$) (figure 6). This may be linked to the intermediate soil moisture of US-Beo. Higher SWC can limit the temperature sensitivity of soil respiration in wetland regions due to the restriction of oxygen and thus, aerobic respiration (Chen *et al* 2018). Alternatively, respiration can be limited by lower SWC through a reduction in microbial mobility and substrate diffusion (Grant and Rochette 1994). The temperature sensitivity of belowground respiration can also be dependent on productivity by providing photosynthates as substrates (Hartley *et al* 2006). This may contribute to US-Bes having the lowest temperature sensitivity, as this site exhibited the lowest productivity (table 2).

Similar studies of annual CO_2 budgets show that the largest annual net CO_2 loss is seen during the non-growing season, particularly associated with early winter respiration (Oechel *et al* 2014, Commane *et al* 2017, Euskirchen *et al* 2017), agreeing with data presented here. As early winter respiration comprises a large part of the CO_2 budget, further increases in zero-curtain duration will likely result in winter CO_2 emissions that exceed growing season uptake (Arndt *et al* 2019b). Each of the sites in this study were found to act as a weak sink for CO_2, yet others have reported relatively strong annual source signals from similar systems (Commane *et al* 2017, Eurskirchen *et al* 2017). This highlights the need for the monitoring and greater representation of mesoscale ($\leqslant$1 km) processes in climate projections, particularly at subgrid scales.

4.2. CH_4 seasonality and annual budget

Growing season CH_4 emissions are lowest at US-Brw (figure 4(b)). This is likely due to lower soil moisture increasing the volume of soil experiencing aerobic conditions not conducive to methanogenesis (Garcia *et al* 2000). The polygon tundra site, US-Beo, had similar CH_4 emissions relative to the inundated US-Bes site despite US-Bes being the site with the higher SWC (figure 4(b)). This may be related to the vegetation community composition. As US-Bes contains a lower percent cover of sedges (Davidson *et al* 2016b), US-Beo may produce more photosynthates,

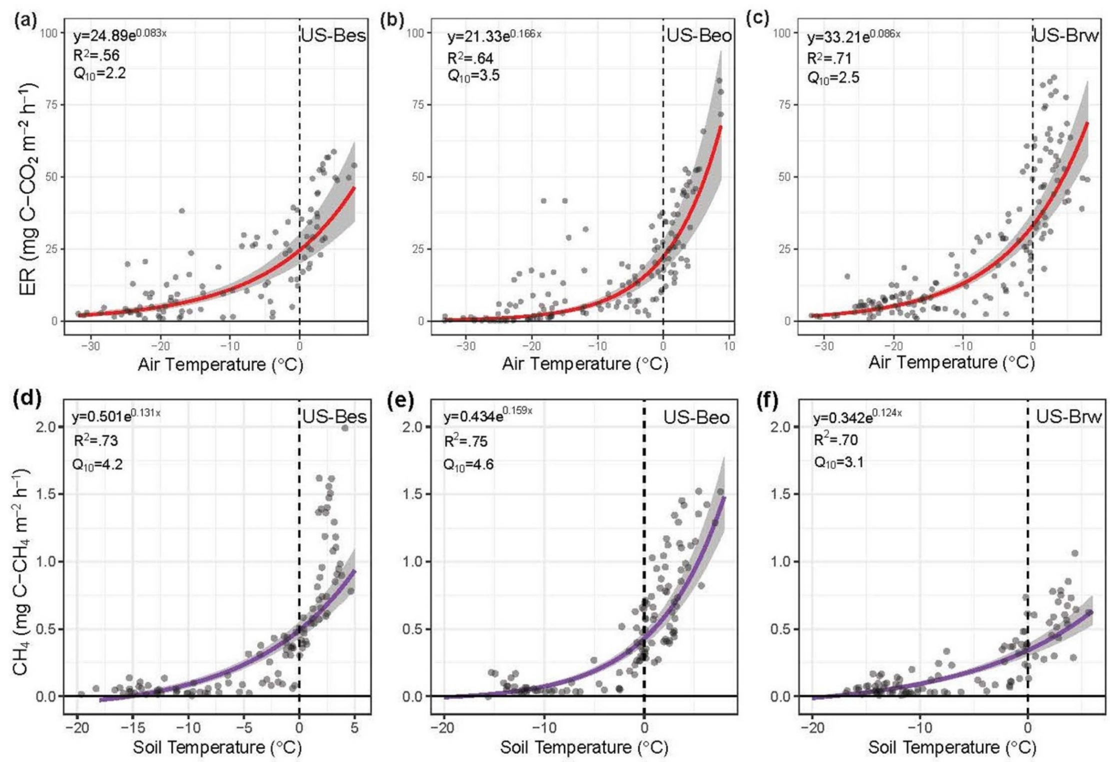

Figure 6. Temperature response curves of ecosystem respiration (ER; (a)–(c) (air temperature)) and CH_4 efflux (d)–(f) (soil temperature)) at US-Bes (a) and (d), US-Beo (b) and (e), and US-Brw (c) and (f). All regressions had a p-value of >0.01.

like acetate, that could leach into surrounding waterlogged soil in polygonal environments, further fueling methanogenesis via acetoclastic methanogenic pathway (King *et al* 2002, Dorodnikov *et al* 2011). Further, sedge density is positively correlated to CH_4 emissions as sedges provide a pathway for CH_4 through the vegetation to the atmosphere (Lai 2009, Andresen *et al* 2017). Interannual variability in CH_4 emissions is low at US-Bes compared with the other sites (figure 5). As US-Bes is consistently inundated, interannual differences in snow melt and rainfall would have a larger impact on SWC and by proxy, oxygen availability at US-Brw, and US-Beo, possibly explaining this variability.

Contrary to zero-curtain CO_2 emission having site dependent variability, zero-curtain CH_4 emissions are roughly equal across all sites. This may be due to the frozen surface soils, creating an ice 'cap', and limiting oxygen diffusion into the soil column thereby equalizing oxygen availability and by extension, methanogenesis, across sites. This shows that variability in the growing season, rather than the zero-curtain, may have a stronger impact on annual CH_4 variability across different landscapes. However, zero-curtain emissions may increase as the zero-curtain extends longer into the winter with a warming climate (Arndt *et al* 2019a). Zero-curtain CH_4 contributions were found to be higher than in previous works due to the length of the study period capturing the range of annual variability (Zona *et al* 2016). Methane temperature response relationships also indicate that temperature dependence was strongest at US-Beo (Q_{10} = 4.6), followed by US-Bes (Q_{10} = 4.2), and US-Brw (Q_{10} = 3.1) (figure 6). As US-Beo, like US-Bes, contains large amounts of anaerobic soil, temperature sensitivity of methane production would be stronger than US-Brw where soil moisture is a limiting factor.

4.3. Annual combined carbon budget

The largest mean combined C emissions were from the mixed landscape US-Beo, exhibiting both inundated and drained areas. These polygonized landscapes comprise close to 65% of the Alaskan coastal plain (Lara *et al* 2018) and contain both anaerobic areas that produce large quantities of CH_4 as well as drained areas where aerobic respiration can readily occur. US-Beo exhibited the strongest temperature response, for both CO_2 and CH_4. On this basis, it is possible that further climate change may disproportionately increase C emissions from polygonized landscapes as rising temperatures will support increased production and emission of CO_2 and CH_4. However, rising temperatures will likely coincide with polygon succession and hydrologic transitions (Liljedahl *et al* 2016). These hydrologic transitions can significantly alter annual carbon budgets (Kittler *et al* 2017), stressing the importance of monitoring landscape heterogeneity for in these regions for carbon budget estimation.

The interplay of CO_2 and CH_4 dynamics are affected strongly by both seasonality and by mesoscale landscape variability. Though the variability in summer C emissions is significant among the landscapes studied, zero curtain releases of CO_2 and CH_4 tend to offset site differences. This acts as a buffer to variability and leads to similar annual combined C budgets across the sites studied. However, the differences in timing and magnitude of CO_2 and CH_4 fluxes elevate the importance of mesoscale processes for restricting uncertainty in Arctic model projections. Arctic regions make up the largest portion of uncertainty in climate global climate models (IPCC 2014). Pan-Arctic models are typically run at coarse scales that describe landscape heterogeneity by the dominant landscape. It has been stressed that a higher degree of spatial and temporal coverage is needed (Natali *et al* 2019) and that representation of wet and dry tundra at a finer scale ($\leqslant$4 km^2) can result in a threefold reduction in model error (Lara *et al* 2020). Data presented here demonstrate the need for this improvement, particularly for models that can represent mesoscale landscape heterogeneity and subsequent differences in seasonal carbon emission patterns.

5. Conclusions

Although the northern coastal tundra region in Alaska continues to be a weak CO_2 sink in all observed landscapes, CH_4 emissions push the region to have a net warming effect on the atmosphere. Data show the site with the largest mean GPP experienced the lowest mean annual CO_2 uptake, while the site with the lowest mean GPP experienced the highest mean annual CO_2 uptake. This is primarily due to zero-curtain CO_2 emissions and indicates that zero-curtain CO_2 emissions are positively correlated with growing season GPP. Despite site variability in growing season CH_4 emissions, zero-curtain CH_4 emissions are nearly equal across sites. This implies that the percent contribution of zero-curtain CH_4 emissions to annual CH_4 budget varies by site and can be larger than previously thought, being as high as 45% of the yearly budget from the zero-curtain period alone and over half of the yearly budget from the total non-growing season (including the zero-curtain). Tundra exhibiting both inundated and drained areas are the largest mean annual combined C source and show a stronger ER and CH_4 temperature response than either largely inundated or drained areas. These results show that local variation in site hydrology, seasonality and interannual variability in regional temperature work in tandem to determine carbon balance. This interaction may be indicative of a variable response under further climate change, yet seemingly lacking the strength to cause strong differences in annual C budgets at this time. As both wetting and drying of Arctic tundra has been reported, differential landscape development in response to climate change and subsequent C budget divergence may occur. Without improved representation of landscape heterogeneity, this potential divergence would likely confound long term global model predictions further, as changes would occur at sub-grid scales.

Data availability statement

The data that support the findings of this study are openly available at the following URL/DOI: https://arcticdata.io/catalog/view/doi:10.18739/A2X34MS1B.

Acknowledgments

This work was funded by the NASA ABoVE Program awarded to Walter C Oechel and Donatella Zona (No. NNX16AF94A) and the National Science Foundation—Office of Polar Programs awarded to Donatella Zona and Walter C Oechel (Nos. 1204263 and 1702797). Additional logistical support was funded by the National Science Foundation—Office of Polar Programs, the NASA ABoVE Program, NOAA CESSRST EPP awarded to Walter C Oechel (No. NA16SEC4810008), the European Union's Horizon 2020 research and innovation program awarded to Walter C Oechel and Donatella Zona (No. 629727890), and from the Natural Environment Research Council (NERC) UAMS Grant awarded to Walter C Oechel and Donatella Zona (No. NE/P002552/1). Geospatial support for this work (figure 1) provided by the Polar Geospatial Center (under NSF OPP Award Nos.1204263 and 1702797). This research was conducted on land owned by the Ukpeaġvik Inupiat Corporation (UIC) whom we thank for their support.

ORCID iDs

Josh Hashemi https://orcid.org/0000-0002-8660-7406
Donatella Zona https://orcid.org/0000-0002-0003-4839
Kyle A Arndt https://orcid.org/0000-0003-4158-2054
Aram Kalhori https://orcid.org/0000-0002-0652-8987

References

Andresen C G, Lara M J, Tweedie C E and Lougheed V L 2017 Rising plant-mediated methane emissions from Arctic wetlands *Glob. Change Biol.* **23** 1128–39

Arndt K A, Lipson D A, Hashemi J, Oechel W C and Zona D 2020 Snow melt stimulates ecosystem respiration in Arctic ecosystems *Glob. Change Biol.* **26** 5042–51

Arndt K A, Oechel W C, Goodrich J P, Bailey B A, Kalhori A, Hashemi J and Zona D 2019b Sensitivity of methane emissions to later soil freezing in Arctic tundra ecosystems *J. Geophys. Res. Biogeosci.* **124** 2595–609

Arndt K A, Santos M, Ustin S L, Davidson S J, Stow D A, Oechel W, Tran T T P, Graybill B and Zona D 2019a Arctic

greening associated with lengthening growing seasons in Northern Alaska *Environ. Res. Lett.* **14** 125018
Birk M A 2020 Respirometry: tools for conducting and analyzing respirometry experiments. R package version 1.1.0 (available at: https://CRAN.R-project.org/package=respirometry)
Chen H, Zou J, Cui J, Nie M and Fang C 2018 Wetland drying increases the temperature sensitivity of soil respiration *Soil Biol. Biochem.* **120** 24–27
Commane R, Lindaas J, Benmergui J, Luus K A, Chang R, Daube B C and Wofsy C 2017 Carbon dioxide sources from Alaska driven by increasing early winter respiration from Arctic tundra *Proc. Natl Acad. Sci.* **114** 5361–6
Davidson S J, Santos M J, Sloan V L, Watts J D, Phoenix G K, Oechel W C and Zona D 2016a Mapping Arctic tundra vegetation communities using field spectroscopy and multispectral satellite data in North Alaska, USA *Remote Sens.* **8** 978
Davidson S J, Sloan V L, Phoenix G K, Wagner R, Fisher J P, Oechel W C and Zona D 2016b Vegetation type dominates the spatial variability in CH_4 emissions across multiple Arctic tundra landscapes *Ecosystems* **19** 1116–32
Dorodnikov M, Knorr K-H, Kuzyakov Y and Wilmking M 2011 Plant-mediated CH_4 transport and contribution of photosynthates to methanogenesis at a boreal mire: a 14C pulse-labeling study *Biogeosciences* **8** 2365–75
Dunfield P, Knowles R, Dumont R and Moore T R 1993 Methane production and consumption in temperate and subarctic peat soils: response to temperature and pH *Soil Biol. Biochem.* **25** 321–6
Euskirchen E S, Bret-Harte M S, Scott G J, Edgar C and Shaver G R 2012 Seasonal patterns of carbon dioxide and water fluxes in three representative tundra ecosystems in northern Alaska *Ecosphere* **3** art4
Euskirchen E S, Bret-Harte M S, Shaver G R, Edgar C W and Romanovsky V E 2017 Long-term release of carbon dioxide from Arctic tundra ecosystems in Alaska *Ecosystems* **20** 960–74
Fox J and Weisberg S 2019 *An R Companion to Applied Regression* 3rd edn (Thousand Oaks, CA: Sage)
Garcia J L, Patel B K C and Ollivier B 2000 Taxonomic, phylogenetic, and ecological diversity of methanogenic Archaea *Anaerobe* **6** 205–26
Goodrich J P, Oechel W C, Gioli B, Moreaux V, Murphy P C, Burba G and Zona D 2016 Impact of different eddy covariance sensors, site set-up, and maintenance on the annual balance of CO_2 and CH_4 in the harsh Arctic environment *Agric. For. Meteorol.* **228–229** 239–51
Grant R F and Rochette P 1994 Soil microbial respiration at different water potentials and temperatures: theory and mathematical modeling *Soil Sci. Soc. Am. J.* **58** 1681–90
Hartley I P, Armstrong A F, Murthy R, Barron-gafford G, Ineson P and Atkin O K 2006 The dependence of respiration on photosynthetic substrate supply and temperature: integrating leaf, soil and ecosystem measurements *Glob. Change Biol.* **12** 1954–68
Hugelius G, Strauss J, Zubrzycki S, Harden J W, Schuur E A G, Ping C-L and Kuhry P 2014 Estimated stocks of circumpolar permafrost carbon with quantified uncertainty ranges and identified data gaps *Biogeosciences* **11** 6573–93
Huissteden J *et al* 2011 Methane emissions from permafrost thaw lakes limited by lake drainage *Nat. Clim. Change* **1** 119–23
Ibrom A, Dellwik E, Flyvbjerg H, Jensen N O and Pilegaard K 2007 Strong low-pass filtering effects on water vapour flux measurements with closed-path eddy correlation systems *Agric. For. Meteorol.* **147** 140–56
IPCC 2014 Climate change 2014: synthesis report *Contribution of Working Groups I, II and III to the Fifth Assessment Report of the Intergovernmental Panel on Climate Change*
Jorgenson M T and Shur Y 2007 Evolution of lakes and basins in northern Alaska and discussion of the thaw lake cycle *J. Geophys. Res. Earth Surface* **112** F02S17
King J Y, Reeburgh W S, Thieler K K, Kling G W, Loya W M, Johnson L C and Nadelhoffer K J 2002 Pulse-labeling studies of carbon cycling in Arctic tundra ecosystems: the contribution of photosynthates to methane emission *Glob. Biogeochem. Cycles* **16** 10-1-10–18
Kirschke S, Bousquet P, Ciais P, Saunois M, Canadell J G, Dlugokencky E J and Zeng G 2013 Three decades of global methane sources and sinks *Nat. Geosci.* **6** 813–23
Kittler F, Heimann M, Kolle O, Zimov N, Zimov S and Göckede M 2017 Long-term drainage reduces CO_2 uptake and CH_4 emissions in a Siberian permafrost ecosystem *Glob. Biogeochem. Cycles* **31** 1704–17
Koch J C, Gurney K and Wipfli M S 2014 Morphology-dependent water budgets and nutrient fluxes in Arctic thaw ponds *Permafr. Periglac. Process.* **25** 79–93
Korman R and Meixner F 2001 An analytical footprint model for non-neutral stratification *Bound.-Layer Meteorol.* **99** 207–24
Kwon H-J, Oechel W C, Zulueta R C and Hastings S J 2006 Effects of climate variability on carbon sequestration among adjacent wet sedge tundra and moist tussock tundra ecosystems *J. Geophys. Res.* **111** G03014
Lai D Y F 2009 Methane dynamics in northern peatlands: a review *Pedosphere* **19** 409–21
Lara M J *et al* 2020 Local-scale Arctic tundra heterogeneity affects regional-scale carbon dynamics *Nat. Commun.* **11** 4925
Lara M J, Nitze I, Grosse G and David McGuire A 2018 Data descriptor: tundra landform and vegetation productivity trend maps for the Arctic Coastal Plain of Northern Alaska *Sci. Data* (https://doi.org/10.1038/sdata.2018.58)
Lasslop G, Reichstein M, Papale D, Richardson A D, Arneth A, Barr A, Stoy P and Wohlfahrt G 2010 Separation of net ecosystem exchange into assimilation and respiration using a light response curve approach: critical issues and global evaluation *Glob. Change Biol.* **16** 187–208
Lawrence D M, Koven C D, Swenson S C, Riley W J and Slater A G 2015 Permafrost thaw and resulting soil moisture changes regulate projected high-latitude CO_2 and CH_4 emissions *Environ. Res. Lett.* **10** 094011
Liljedahl A K, Boike J, Daanen R P, Fedorov A N, Frost G V, Grosse G and Zona D 2016 Pan-Arctic ice-wedge degradation in warming permafrost and its influence on tundra hydrology *Nat. Geosci.* **9** 312–8
Maglione P, Parente C and Vallario A 2014 Coastline extraction using high resolution WorldView-2 satellite imagery *Eur. J. Remote Sens.* **47** 685–99
Martin A F, Lantz T C and Humphreys E R 2018 Ice wedge degradation and CO_2 and CH_4 Northwest Territories *Arct. Sci.* **4** 130–45
Mauder M and Foken T 2011 Documentation and instruction manual of the eddy-covariance software package TK3 vol 46 (Bayreuth)
McGuire A D, Christensen T R, Hayes D, Heroult A, Euskirchen E, Kimball J S and Yi Y 2012 An assessment of the carbon balance of Arctic tundra: comparisons among observations, process models, and atmospheric inversions *Biogeosciences* **9** 3185–204
Megonigal J P and Schlesinger W H 2002 Methane-limited methanotrophy in tidal freshwater swamps *Glob. Biogeochem. Cycles* **16** 1088
Natali S M, Schuur E A G, Mauritz M, Schade J D, Celis G, Crummer K G and Webb E E 2015 Permafrost thaw and soil moisture driving CO_2 and CH_4 release from upland tundra *J. Geophys. Res. Biogeosci.* **120** 1–13
Natali S M, Watts J D, Rogers B M, Potter S, Ludwig S M, Selbmann A-K and Zona D 2019 Large loss of CO_2 in winter observed across the northern permafrost region *Nat. Clim. Change* **9** 852–7 8–019–0592–8
Nielsen C S, Hasselquist N J, Nilsson M B, Öquist M, Järveoja J and Peichl M 2019 A novel approach for high-frequency *in-situ* quantification of methane oxidation in Peatlands *Soil Syst.* **3** 4
Oechel W C, Laskowski C A, Burba G, Gioli B and Kalhori A A M 2014 Annual patterns and budget of CO_2 flux in an Arctic tussock tundra ecosystem *J. Geophys. Res. Biogeosci.* **119** 323–39

Outcalt S I, Nelson F E and Hinkel K M 1990 The zero-curtain effect: heat and mass transfer across an isothermal region in freezing soil *Water Resour. Res.* **26** 1509–16

R Core Team 2019 R: a language and environment for statistical computing *Vienna, Austria: R Foundation for Statistical Computing* accepted (available at: www.R-project.org/)

Reichstein M *et al* 2005 On the separation of net ecosystem exchange into assimilation and ecosystem respiration: review and improved algorithm *Glob. Change Biol.* **11** 1424–39

Schuur E A G, Abbott B W, Bowden W B, Brovkin V, Camill P, Canadell J G and Zimov S A 2013 Expert assessment of vulnerability of permafrost carbon to climate change *Clim. Change* **119** 359–74

Serreze M C and Francis J A 2006 The Arctic amplification debate *Clim. Change* **76** 241–64

Tamocai C, Canadell J G, Schuur E A G, Kuhry P, Mazhitova G and Zimov S 2009 Soil organic carbon pools in the northern circumpolar permafrost region *Glob. Biogeochem. Cycles* **23** 1–11

Taylor M A, Celis G, Ledman J D, Bracho R and Schuur E A G 2018 Methane efflux measured by eddy covariance in Alaskan upland tundra undergoing permafrost degradation *J. Geophys. Res. Biogeosci.* **123** 2695–710

Tian H, Lu C, Chen G, Tao B, Pan S, del Grosso S and Prior S A 2012 Contemporary and projected biogenic fluxes of methane and nitrous oxide in North American terrestrial ecosystems *Front. Ecol. Environ.* **10** 528–36

Treat C C, Bloom A A and Marushchak M E 2018a Nongrowing season methane emissions-a significant component of annual emissions across northern ecosystems *Glob. Change Biol.* **24** 3331–43

Treat C C *et al* 2018b Tundra landscape heterogeneity, not interannual variability, controls the decadal regional carbon balance in the Western Russian Arctic *Glob. Change Biol.* **24** 5188–204

Webber P J 1978 Spatial and temporal variation of the vegetation and its production, Barrow, Alaska *Vegetation and Production Ecology of an Alaskan Arctic Tundra* ed L L Tieszen (New York: Springer) 37–112

Wilczak J M, Oncley S P and Stage S A 2001 Sonic anemometer tilt correction algorithms *Bound.-Layer Meteorol.* **99** 127–50 66204465

Wutzler T, Lucas-Moffat A, Migliavacca M, Knauer J, Sickel K, Šigut L and Reichstein M 2018 Basic and extensible post-processing of eddy covariance flux data with REddyProc *Biogeosciences* **15** 5015–30

Xenakis G 2016 FREddyPro: post-processing EddyPro full output file. R package version 1.0

Zimov S A, Schuur E A G and Stuart Chapin F 2006 Permafrost and the global carbon budget *Science* **312** 1612–3

Zona D, Gioli B, Commane R, Lindaas J, Wofsy S C, Miller C E and Oechel W C 2016 Cold season emissions dominate the Arctic tundra methane budget *Proc. Natl Acad. Sci.* **113** 40–45

Zulueta R C, Oechel W C, Loescher H W, Lawrence W T and Paw U K T 2011 Aircraft-derived regional scale CO_2 fluxes from vegetated drained thaw-lake basins and interstitial tundra on the Arctic Coastal Plain of Alaska *Glob. Change Biol.* **17** 2781–802